Mitigation of Over-Frequency through Optimal Allocation of BESS in a Low-Inertia Power System

Nahid-Al Masood [1,*] **, Md. Nahid Haque Shazon** [1] **, Hasin Mussayab Ahmed** [1] **and Shohana Rahman Deeba** [2]

1   Department of EEE, Bangladesh University of Engineering and Technology, Dhaka 1205, Bangladesh;
     shazon.buet.eee@gmail.com (M.N.H.S.); punnohasin@gmail.com (H.M.A.)
2   Department of Electrical and Computer Engineering, North South University, Dhaka 1229, Bangladesh;
     shohana.deeba@northsouth.edu
*   Correspondence: n.masood@uq.edu.au; Tel.: +880-171-649-4885

Abstract: The primary objective of this paper is to alleviate the over-frequency problem in low-inertia power systems through optimal allocation of a Battery Energy Storage System (BESS). With prolific integration of wind power, conventional fossil-fuel driven synchronous generators are being replaced in the generation fleet. Variable speed wind machines are connected to the grid via power electronics converters. As such, these machines usually do not participate in frequency regulation. During high wind penetration, a generation-rich zone of an interconnected power system may face significant over-frequency following the loss of interconnection. If the frequency goes above a certain threshold, an Over-Frequency Generator Shedding (OFGS) scheme is activated. This may cause considerable amount of generation cut in a low-inertia power system. To address this challenge, this paper develops a siting and sizing methodology of frequency-responsive BESS to simultaneously maintain frequency and voltage stabilities. As such, BESS is placed at the most voltage-sensitive bus, determined by an index called reactive power margin. Furthermore, an optimization model is formulated to determine the BESS size to avoid generation shedding. The proposed technique is applied to a low-inertia power system, which resembles the equivalent high-voltage transmission network of South Australia. The simulation results reveal that the developed methodology successfully mitigates the over-frequency phenomenon. In addition, the proposed technique is found to be more effective than its counterpart (i.e., without BESS) to enhance the frequency resilience of a low-inertia grid.

Keywords: over-frequency; low-inertia power system; frequency response; battery energy storage system; voltage stability

1. Introduction

Interconnections between adjacent zones in a power system are erected to ensure economic and reliable operation [1]. During significant amount of power export from a generation-rich area to its neighboring zone, a loss of interconnection can cause an excessive rise in system frequency in the power-exporting zone [2]. In conventional power systems where sufficient numbers of synchronous generators are committed, a sudden increase in frequency can be stopped via inertia and governor responses [3]. However, due to the increased penetration of wind generation, conventional synchronous generators are being replaced in the generation mix [4,5]. Modern wind power plants predominantly deploy Type-III (Doubly Fed Induction generator (DFIG)) and Type-IV (Full Scale Converter (FSC)) wind turbine generators (WTGs). These WTGs are interfaced with the grid via power electronic converters, which decouple them from the corresponding network [6]. Consequently, these machines usually do not offer inertia and governor response to control system frequency [7]. Therefore, under

high wind penetration, maintaining an adequate frequency response is becoming challenging due to the presence of a few synchronous generators in a low-inertia grid.

Following the loss of an interconnection in a low-inertia grid under power export conditions, network frequency can go above a certain threshold [8]. As a result, over-frequency relays disconnect the online generators [9]. Consequently, cascading tripping of generators may take place, which eventually can cause a significant amount of generation loss. Therefore, the mitigation of over-frequency is a vital concern to enhance frequency resilience. To this end, a number of strategies are reported in the literature to address this issue. An over-frequency mitigation scheme via the tripping of generators located close to the disturbance is suggested in [10]. Furthermore, an Over-Frequency Generator Shedding (OFGS) technique is proposed in [11], where coordination is preserved between the over-speed protection controller and generator shedding relays. Furthermore, an active power reduction scheme of virtual power plants aided by a decision tree strategy is reported in [12]. Similarly, active power reduction from a distributed generator for over-frequency management is given emphasis for an islanded microgrid in [13,14]. In addition, for conventional power systems, grid connected wind farm shedding is found to be effective to arrest frequency rise [15]. Notably, the rapid response time of the Battery Energy Storage System (BESS) enables it to be used for frequency control as it can supply or absorb active power following a disturbance. However, the deployment of BESS for over-frequency mitigation is overlooked in the current literature.

BESS has been predominantly utilized in power systems for various applications viz. variability and intermittency reduction in renewable sources, power quality and reliability improvement, load leveling, peak shifting, valley filling, increasing spinning reserves and so on [16,17]. In addition, BESS can be placed in microgrids with higher renewable penetration for active power sharing [18]. Siting and sizing strategies of BESS for reducing daily production cost in a renewable integrated power system are investigated in [19]. Moreover, network congestion reduction is accomplished by the optimal sizing and placement of BESS in [20]. For providing a primary frequency response in a Mexican transmission network, a BESS allocation strategy is proposed in [21]. In [22], a BESS sizing methodology is developed by determining energy and power ratings to provide an inertial response as well as a primary frequency response in a wind-dominated power grid. A BESS sizing methodology is presented in [23] using grid voltage code violation as a limiting criterion. Likewise, an optimized BESS capacity is determined in [24] and validated through measurement data. Optimal placement of energy storage is reported in [25] by using the alternating direction method of multipliers algorithm for providing ancillary service in a power system. Optimal siting and sizing of a distributed energy storage system is specified using bi-level optimization in [26] for mitigating the voltage impact of solar photovoltaic (PV) in a distribution system. An AC optimal power flow method and linearized DC power flow approximation method are utilized in [27,28] to find the most appropriate allocation strategy of BESS.

Conventionally, power systems rely on an OFGS scheme to mitigate over-frequency events. However, this causes a certain amount of generation loss. To avert generator shedding (i.e., to avoid the activation of the OFGS scheme), deployment of BESS can be a prudent choice. However, BESS is expensive; hence, its size needs to be appropriately determined to minimize financial concerns. Furthermore, proper siting of BESS can ensure voltage stability, which is an additional advantage for network operators. In the literature, a significant number of studies are carried out to investigate the optimal siting and sizing of BESS from various perspectives. However, none of the existing works report any strategies for the optimal allocation of BESS to resolve the over-frequency problem in a low-inertia grid. To address this important yet unexplored research gap, this paper aims to make the following contributions.

- An optimal sizing approach for frequency-responsive BESS is developed to mitigate the risk of over-frequency and subsequent generator shedding in a low-inertia power system under high wind power penetration.

- Frequency deviation is utilized as an objective function in the optimization formulation, whereas Rate of Change of Frequency (ROCOF) and BESS State of Charge (SoC) are considered as constraints in the optimization formulation. Thus, both frequency response parameters and battery charging limits are taken into account while evaluating the optimal BESS size.
- A siting strategy of BESS is utilized to take care of voltage stability besides frequency response adequacy. To this end, BESS is placed at the weakest bus using a voltage stability index called reactive power margin.
- The proposed methodology is applied to a low-inertia test network, which represents the equivalent high-voltage transmission network of South Australia. The effectiveness of the proposed approach is demonstrated via dynamic simulations following a large contingency in various wind penetration cases. Moreover, the developed technique is validated by comparing the frequency response performances using with BESS and without BESS strategies.

It is to be clarified that the proposed approach is complementary to frequency reserves. To this end, a symmetric primary frequency control reserve (FCR) is considered in this paper. As such, following an over-frequency event, power outputs of synchronous generators decrease via governor action. However, in a low-inertia system, a few synchronous generators are committed in the grid. Therefore, the amount of FCR is not adequate to stop the frequency rise following a large contingency. Consequently, the frequency may go above the OFGS threshold. It could cause the loss of a certain amount of generation. To avert such a situation, BESS is deployed along with FCR to keep the system frequency below the OFGS activation threshold.

The rest of the paper is organized as follows. Section 2 describes the proposed methodology supported by the necessary theoretical background. Section 3 contains the simulation network and simulation scenarios. Section 4 presents comprehensive simulation results, analyses, validation and other aspects of the proposed techniques. Finally, Section 5 summarizes the key findings to conclude the paper.

2. Methodology

Prior to finding the optimal size, the most appropriate location to connect a BESS needs to be determined. The placement should be such that the BESS retains voltage stability apart from alleviating the over-frequency phenomenon. As such, a siting strategy of BESS is presented first. Then, the optimal size of frequency-responsive BESS is determined using the Particle Swarm Optimization (PSO) technique.

2.1. Siting Strategy of BESS

BESS is connected to the weakest bus of a network so that it can provide additional support to retain voltage stability following a contingency. In this paper, reactive power margin is used as an index to identify the weakest bus. In the following sub-sections, the fundamental concept and computation algorithm of reactive power margin are discussed.

2.1.1. Basics of Reactive Power Margin

Reactive power margin is quantified by the MVAr distance between the minimal point of a reactive power vs. voltage (Q–V) curve and its voltage axis, as demonstrated in Figure 1 [29,30]. This minimal point refers to the proximity to voltage collapse of a load bus. The complete Q–V curve can be produced by a continuation method [31,32].
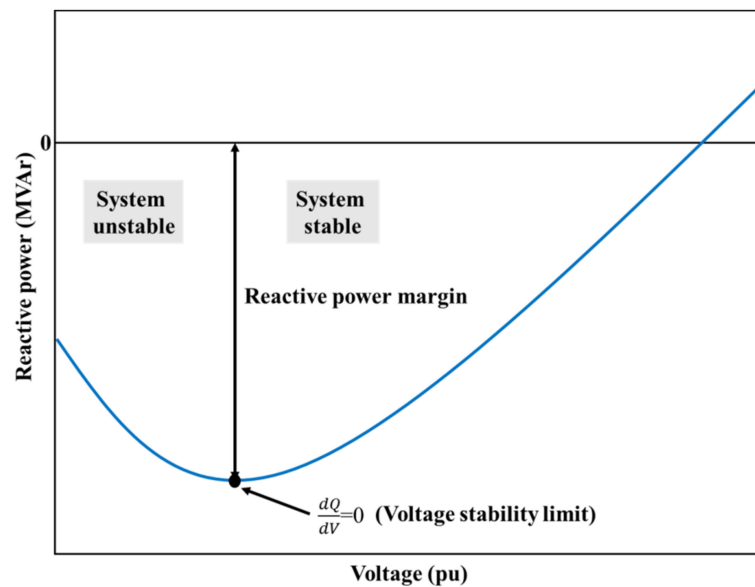
Figure 1. A typical reactive power vs. voltage (Q–V) curve at a load bus

A power system with numerous generators and loads can be equivalently represented by a 'single source and single load bus' system, as shown in Figure 2 [33]. From Figure 2, at the load bus, real and reactive power can be represented by Equation (1).

$$P_L + jQ_L = \frac{\overline{V_L}\left(\overline{V_G} - \overline{V_L}\right)^*}{\overline{Z}} \tag{1}$$

where P_L is the real power (in p.u), Q_L is the reactive power (in p.u), $\overline{V_G}$ is the phasor voltage at generator bus (in p.u), $\overline{V_L}$ refers to the phasor voltage at load bus and $\overline{Z}$ denotes the transmission line impedance in phasor form (in p.u). Generator bus voltage and load bus voltage can be expressed using Equations (2) and (3), respectively.

$$\overline{V_G} = V_G e^{j\delta_G} \tag{2}$$

$$\overline{V_L} = V_L e^{j\delta_L} \tag{3}$$

where V_G and V_L are generator bus voltage magnitude and load bus voltage magnitude (in p.u), respectively. Furthermore, δ_G and δ_L refer to generator bus voltage angle and load bus voltage angle, respectively (in rad.).
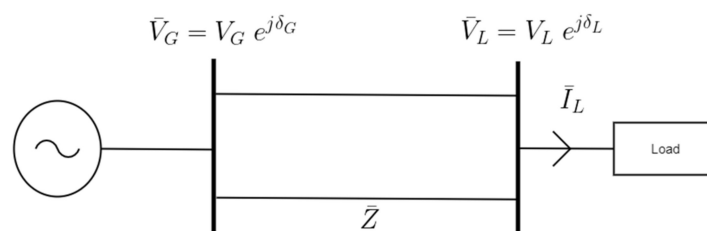

Figure 2. Equivalent two-bus system [33].

The relationship between real and reactive power at the load bus is given by Equation (4).

$$Q_L = P_L \tan \phi \tag{4}$$

where ϕ denotes the power factor angle at load bus (in rad). Let us assume that transmission line impedance $\overline{Z}$ is written by Equation (5). Thus, expressions of real and reactive power can be further expanded and written via Equations (6) and (7).

$$\overline{Z} = R + jX \tag{5}$$

$$\left(R^2 + X^2\right)(1 \; + \; \tan^2 \phi)P_L^2 \; + \; 2V_L^2 P_L(R + X \tan \phi) \; + \; \left(V_L^4 - V_G^2 V_L^2\right) \; = \; 0 \tag{6}$$

$$\left(R^2 + X^2\right)(1 + \tan^2 \phi)Q_L^2 \; + \; 2V_L^2 Q_L(R + X \tan \phi) \; + \; \left(V_L^4 - V_G^2 V_L^2\right) \; = \; 0 \tag{7}$$

where R and X refer to the transmission line resistance (in p.u) and reactance (in p.u), respectively. Thus, Q–V curve can be achieved by solving Equations (6) and (7). However, near the lowest point (i.e., the voltage collapse point) of the Q–V curve, the Jacobian matrix becomes singular and, consequently, obtaining numerical solution becomes difficult. As the continuation power flow method overcomes this singularity problem in the vicinity of a voltage collapse point, this method can be utilized for achieving a complete Q–V curve [34].

2.1.2. Continuation Power Flow Method

The continuation power flow method eliminates the singularity problem near the voltage stability limit point. It does so by generating a complete voltage profile through automatic variation in the loading parameter λ. The method is depicted in Figure 3 [34], where the initial equilibrium state is denoted by (z_1, λ_1). An initial guess $(z_1 + \Delta z_1)$ is generated by predictor step $\Delta\lambda_1$, where Δz_1 is the direction vector. A new equilibrium point (z_2, λ_2) is determined afterwards using a parameterization technique in the continuation method.
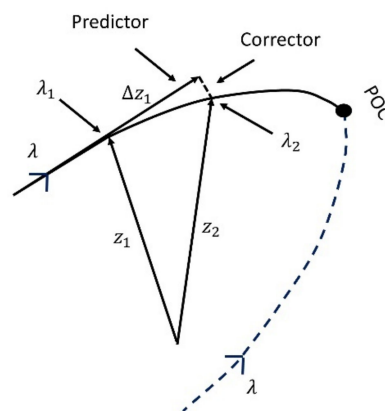

Figure 3. Illustration of continuation method [34].

Assume that a typical quasi-state model of a power system is expressed by the functional relationship shown by Equation (8). Then, the fundamental equation for sensitivity analysis at an equilibrium point (z_1, λ_1) is given by Equation (9).

$$\begin{bmatrix} \dot{x} \\ 0 \end{bmatrix} \; = \; F(z, \lambda) \tag{8}$$

$$\frac{\partial F}{\partial z}dz + \frac{\partial F}{\partial \lambda}d\lambda \; = \; 0 \tag{9}$$

where $z = [x \; y]^T$, x is the vector of state variables, y is the vector of algebraic variables and λ is the time dependent loading parameter. The tangent vector at equilibrium point 1 can be obtained by modifying

Equation (9). Normalization of this vector yields parameter change, which can be expressed using Equation (10).

$$\Delta\lambda_1 = \frac{k}{\left|\frac{dz}{d\lambda}(z_1,\lambda_1)\right|} \tag{10}$$

where k is a scalar with a positive value, which controls the predictor step $\Delta\lambda_1$. Then, the direction vector Δz_1 can be measured using Equation (9).

$$\Delta z_1 = \Delta\lambda_1 \frac{dz}{d\lambda}_{(z_1,\lambda_1)} \tag{11}$$

Using Equations (10) and (11), a new initial guess can be achieved. Finally, by using predictor step and initial guess, an actual point in the system profile can be computed by solving Equations (12) and (13).

$$F(z,\lambda) = 0 \tag{12}$$

$$\rho(z,\lambda) = 0 \tag{13}$$

Note that Equation (12) corresponds to the system state equations, which in this case are power flow equations. In addition, Equation (13) refers to a phase condition that ensures the non-singularity of the system Jacobian matrix at the bifurcation point (i.e., voltage collapse point).

2.2. Sizing Strategy of BESS

In this sub-section, at first, a frequency-responsive BESS model is introduced. Then, the optimal size of a BESS is determined to reconcile the over-frequency challenge.

2.2.1. Frequency Responsive Model of BESS

To design a frequency-responsive BESS, the EPRI (Electric Power Research Institute) CBEST model [35] is taken into account in this research work. BESS is integrated into the grid via a voltage-source converter. The active power control strategy of BESS, depending on frequency deviation, is illustrated in Figure 4. In this figure, P_{init} refers to the initial active power of BESS (in p.u), P_{max} denotes the maximum power limit (in p.u) and MBASE means the system base MVA. Battery terminal voltage and converter current limit are denoted by V_{AC} and I_{ACMAX}, respectively.
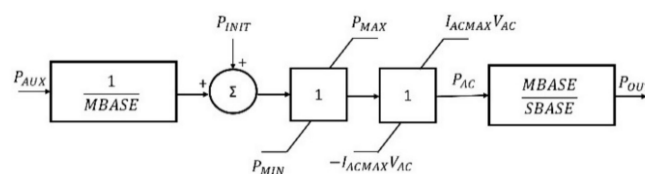

Figure 4. Active power control of Battery Energy Storage System (BESS).

A frequency-sensitive auxiliary power signal P_{AUX} is used to control BESS active power. This auxiliary power signal is triggered by any deviation in system frequency. The auxiliary power signal generator block is illustrated in Figure 5. It consists of a low pass filter, time delay, gain and max–min limiter blocks.
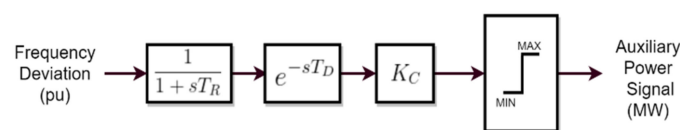

Figure 5. Frequency sensitive auxiliary power signal model.

Following a frequency deviation (drop/rise), an auxiliary signal is generated. Consequently, this signal increases/decreases the active power output of BESS. Such a change in BESS active power output eventually regulates the system frequency.

2.2.2. Optimal Sizing of Frequency-Responsive BESS

The main objective of BESS sizing is to minimize frequency deviation following a large disturbance so that the over-frequency issue is resolved. To this end, an optimization problem is formulated where the objective function (*OF*) includes frequency deviation. Note that the frequency deviation is a function of time and BESS size. The target is to minimize the objective function, subject to some constraints. The main constraints are system ROCOF (i.e., df/dt), BESS size and the SoC of BESS.

The objective function is expressed by Equation (14).

$$OF = \Delta f(t, P_b) \tag{14}$$

where $\Delta f(t, P_b)$ is the maximum frequency deviation from the nominal frequency. Here, t is the time and P_b is the optimization variable, which is BESS size (in MW).

Thus, the optimization problem can be formulated using Equations (15)–(18).

$$\min_{P_b} OF(t, P_b) \tag{15}$$

subject to

$$ROCOF^{min} \le |ROCOF| \le ROCOF^{max} \tag{16}$$

$$P_{BESS}{}^{min} \le P_{BESS} \le P_{BESS}{}^{max} \tag{17}$$

$$(SoC_{BESS})^{min} \le |SoC| \le (SoC_{BESS})^{max} \tag{18}$$

Equation (16) ensures that system ROCOF after a disturbance does not surpass maximum and minimum limits. In this paper, the minimum and maximum acceptable ROCOFs are assumed to be $ROCOF_{min} = -1.0$ Hz/s and $ROCOF_{max} = +1.0$ Hz/s [36]. In addition, Equation (17) confirms that BESS power output stays within the predefined limits P_{BESS}^{min} and P_{BESS}^{max}. These limits can be set by a system operator. Moreover, SoC during charging and discharging is retained within acceptable limits following Equation (18).

To find the most appropriate BESS size, the Particle Swarm Optimization (PSO) is applied in this research work [37]. The PSO algorithm is instigated by initializing m number of random swarm particles. These random particles have R number of unknown parameters to be optimized and each particle corresponds to a probable solution. A random velocity is assigned to each particle and then this particle is flown through the problem space. Each particle has the ability to retain memory and keeps track of its former best position (*Pbest*) and fitness. The particles with best fitness are termed the global best (*Gbest*) of the swarm.

The basic aim of the PSO algorithm is to accelerate each particle in the direction of its *Pbest* and *Gbest* locations. At each time step, the acceleration is weighted with a random number. The velocity and position of each particle alters according to Equations (19) and (20).

$$v_{id}(m) = wv_{id}(m-1) + acc_1 rand_1 (Gbest - P_{id}(m-1)) + acc_2 rand_2 (Pbest_i - P_{id}(m-1)) \tag{19}$$

$$P_{id}(m) = P_{id}(m-1) + V_{id}(m) \tag{20}$$

where v_{id} means the velocity of particle i and P_{id} refers to the position of particle i in a d dimensional space for m-th iteration. The particles are accelerated by acc_1 and acc_2 towards $Pbest_i$ and *Gbest* positions. Furthermore, w denotes the velocity scaling factor, which is a weightage with a value $\epsilon(0, 1)$. In addition, $rand_1$ and $rand_2$ are random numbers with a value between 0 and 1 [38].

For better understanding, the PSO technique is stepwise described as follows. Figure 6 illustrates the steps via a flowchart.

Step 1: Model the low-inertia power system and initialize PSO parameters.

Step 2: Form a random matrix to initialize the position and velocity of the swarm particles by considering given constraints.

Step 3: Evaluate the objective function by determining minimum error.

Step 4: Update the *Pbest* and *Gbest* for each particle.

Step 5: Using the new local and global best, update the velocity and position of each particle.

Step 6: Check whether the termination criterion is fulfilled. The process is stopped if the termination condition is fulfilled. If not, the process returns to Step-2 and we initialize the particles' velocities with new random numbers. When the change in objective function for consecutive iterations is less than 1×10^{-8}, it is considered that the termination criterion is met. Furthermore, if the maximum iteration number is reached, the process is terminated as well. In this paper, the maximum iteration number is assumed to be 100.
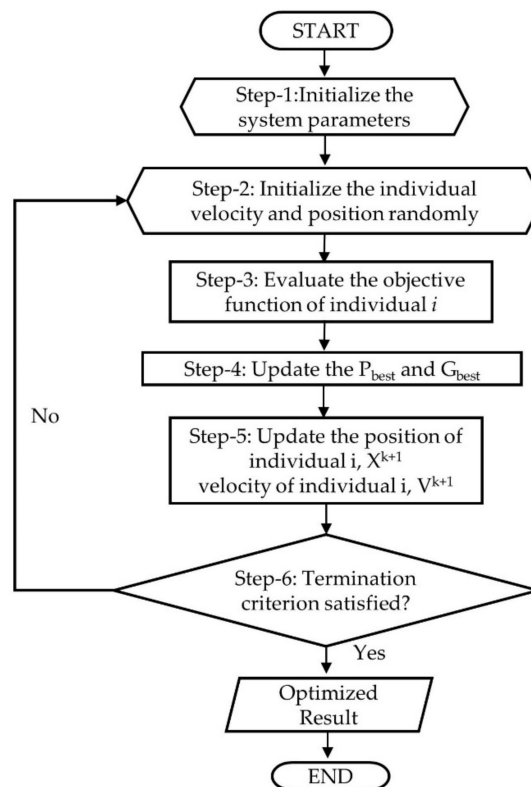
Figure 6. Flowchart of optimization process.

3. Simulation Network and Scenarios

3.1. Simulation Network

The proposed siting and sizing methodology of BESS is applied to a test network. The network is formed based on the 14-Generator Model of South-East Australia [39]. The test network consists of two areas viz. Area-A and Area-B. Area-A resembles the high-voltage transmission network of South Australia. Note that South Australia is a typical example of a low-inertia grid due to high wind power penetration. In addition, Area-B represents the adjacent state, Victoria, which is connected to South Australia via a 275 kV high-voltage AC interconnection. The simulation network is depicted in

Figure 7. Area-B is further connected to the rest of the Australian states, which are not shown here for simplicity.
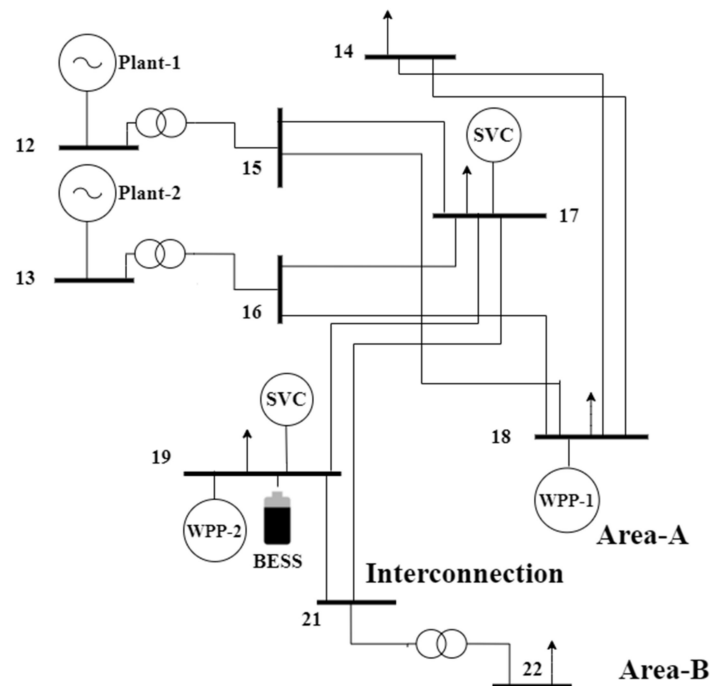

Figure 7. Single-line diagram of the test network.

Two conventional power plants, namely Plant-1 and Plant-2 are present in Area-A. Both power plants consist of multiple generating units. Table 1 outlines the nameplate data of these conventional power plants.

Table 1. Nameplate data of conventional power plants.

Power Plant Name	No. of Available Units	Rated Capacity of Each Unit (MW)	Rated MVA of Each Unit (MVA)	Inertia Constant of Each Unit (s)
Plant-1	4	200	250.00	4.0
Plant-2	6	150	166.67	7.5

The wind power plants are connected to two places—bus 18 and bus 19 (denoted as WPP-1 and WPP-2). These buses are chosen based on the actual geographical locations of South Australian wind power plants. Type-3 WTGs are utilized to model the wind power plants. The total load in Area-A is assumed to be 1500 MW during simulations. Moreover, the total power generation from conventional and wind power plants are higher than that of total load in Area-A. Thus, Area-A is a generation-rich zone and it exports power to Area-B via interconnection. Furthermore, a BESS is placed at bus 19 using the proposed siting methodology (detailed analysis is given in Section 4).

3.2. Simulation Scenarios

For simulating the over-frequency situation, a loss of interconnection under the power export condition (from Area-A to Area-B) is considered as a contingency. To investigate the effectiveness of the proposed methodology, three different case studies are considered. These are as follows: trip of 400-MW interconnection (case-1), trip of 450-MW interconnection (case-2) and trip of 500-MW interconnection (case-3). Note that the interconnection between Area-A (which refers to South Australia) and Area-B (which refers to Victoria) is known as the Heywood interconnection. This interconnection has a nominal

capacity of 500 MW when exporting power from Area-A to Area-B [40]. Furthermore, to investigate the survivability of the studied low-inertia grid under worst-case conditions, high contingency scenarios are analyzed. Therefore, three cases (viz. loss of 400 MW, 450 MW and 500 MW) around the nominal capacity of the interconnection are simulated.

In each case, the number of committed synchronous generators is varied from five to three. As such, the range of total inertia becomes 5500–3500 MWs. The system load is kept unchanged at 1500 MW for all cases. In addition, wind generation changes from 1350 MW to 1800 MW in Area-A. All the simulations are executed in PSS®E software [41], which is widely used in industry and academia to perform power system studies. The simulation scenarios are summarized in Table 2.

Table 2. Simulation scenarios.

Case Study	Contingency Size (MW)	No. of Online Synchronous Generators	Synchronous Generation (MW)	Wind Generation (MW)	Inter-Connection Flow (MW)
1	400	5	662	1350	400
		4	523	1500	400
		3	386	1650	400
2	450	5	666	1400	450
		4	526	1550	450
		3	389	1700	450
3	500	5	676	1500	500
		4	535	1650	500
		3	397	1800	500

When system frequency rises over a certain threshold, the OFGS scheme is activated to reestablish load–generation balance. As mentioned before, the low-inertia test network represents the equivalent high-voltage transmission network of South Australia. To this end, the grid code of the Australian National Electricity Market is taken into account. According to this grid code [42], 51 Hz is considered as the threshold for over-frequency management. Therefore, the OFGS scheme is activated when the system frequency exceeds 51 Hz.

The optimal size of BESS is determined following the loss of 450 MW interconnection to avoid OFGS. In other words, by incorporating BESS, system frequency is restricted below 51 Hz so that no generator shedding takes place. Thus, the 450 MW interconnection trip is assumed to be the baseline contingency to evaluate BESS size. Afterwards, the frequency response is analyzed for the aforementioned three cases (refer to Table 2) when the optimally sized BESS is allocated in Area-A.

4. Results and Analyses

4.1. Siting and Sizing of BESS

At first, the most appropriate location to place a frequency-responsive BESS is investigated. To this end, reactive power margins of different load buses are calculated from Q–V curves constructed using the continuation power flow method. The values are given in Table 3. It can be seen that bus 19 has the lowest reactive power margin. It implies that this bus refers to the weakest bus in Area-A in terms of voltage stability. Therefore, bus 19 is selected as the best location to connect the BESS to take care of voltage stability after a contingency.

Table 3. Reactive power margin of load buses.

Bus Number	Reactive Power Margin (MVAr)
14	745.08
17	648.10
18	874.04
19	270.73

Next, to find the optimal size of BESS, the optimization model stated in Section 2 is solved using the PSO algorithm. For the 450 MW contingency, the optimal size of BESS is found to be 115 MW. Therefore, a 115-MW BESS is placed at bus 19 to avoid the shedding of generators due to over-frequency. Note that, for 400 MW and 500 MW contingencies, system performance is also evaluated with this 115-MW BESS.

4.2. Mitigation of Over-Frequency

To explore the performance of the proposed methodology, the frequency response is analyzed in various contingency cases. Following the loss of interconnection, the frequencies of committed synchronous generators are noted. Then, the center of frequency (f in Hz) is calculated by Equation (21). This equation is adopted to eliminate small variations in measured frequencies.

$$f = \frac{\sum_{i=1}^{i=n}(f_i \times S_i \times H_i)}{\sum_{i=1}^{i=n}(S_i \times H_i)} \tag{21}$$

where f_i refers to the frequency of the i-th synchronous generator (in Hz), S_i denotes the MVA rating of the i-th synchronous generator and H_i is the inertia constant of the i-th synchronous generator (in s). The alleviation of the over-frequency phenomenon through optimally sized BESS in different cases is investigated in the following subsections.

4.2.1. System Performance in Case-1

In this case, the 400-MW interconnection trip under power export conditions (from Area-A to Area-B) is applied as a contingency. Following this event, system frequency in Area-A starts to increase. This deviation in frequency (from nominal value) triggers the auxiliary power signal of the BESS. Consequently, the BESS is activated and absorbs power. As a result, load–generation balance in Area-A is reestablished, and the frequency incline is stopped before the OFGS scheme is activated.

Frequency response along with BESS output power curves for different numbers of committed synchronous generators are illustrated in Figures 8–10. The negative sign in BESS output curves implies power absorption. It can be seen that the frequency peaks (also referred to as frequency summits in this paper) are 50.74 Hz, 50.81 Hz and 50.83 Hz in five-machine, four-machine and three-machine cases, respectively. Corresponding ROCOFs are found to be 0.88 Hz/s, 0.90 Hz/s and 0.92 Hz/s, respectively. Therefore, system frequency remains below 51 Hz and ROCOF becomes less than 1 Hz/s in all cases. Hence, the over-frequency challenge is successfully addressed using the proposed methodology.
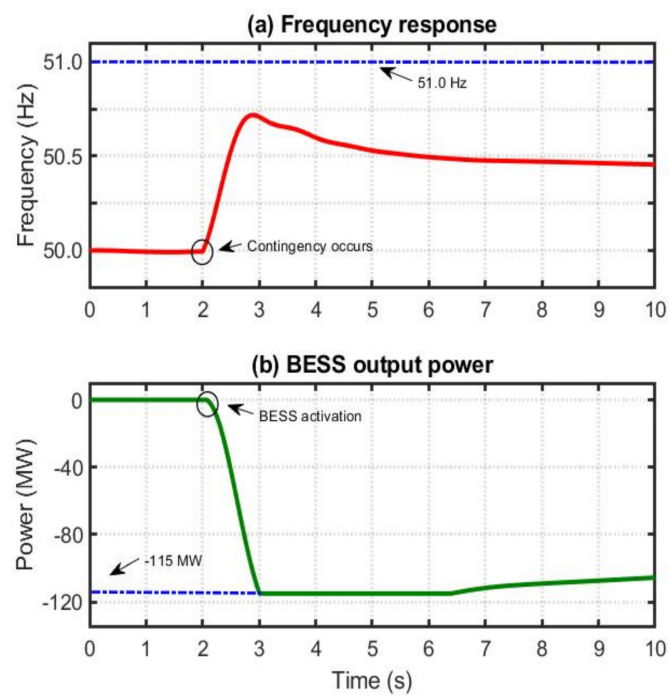
Figure 8. Frequency responses and BESS output due to 400-MW interconnection trip in five-machine case.
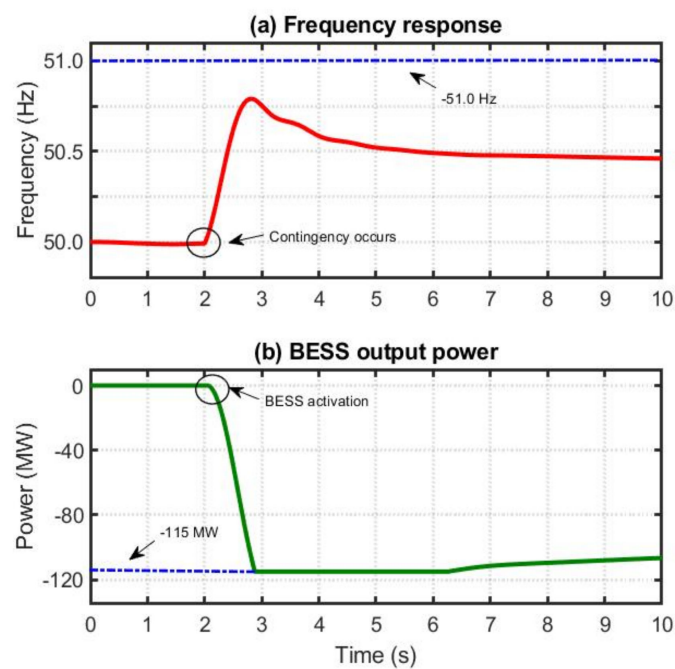

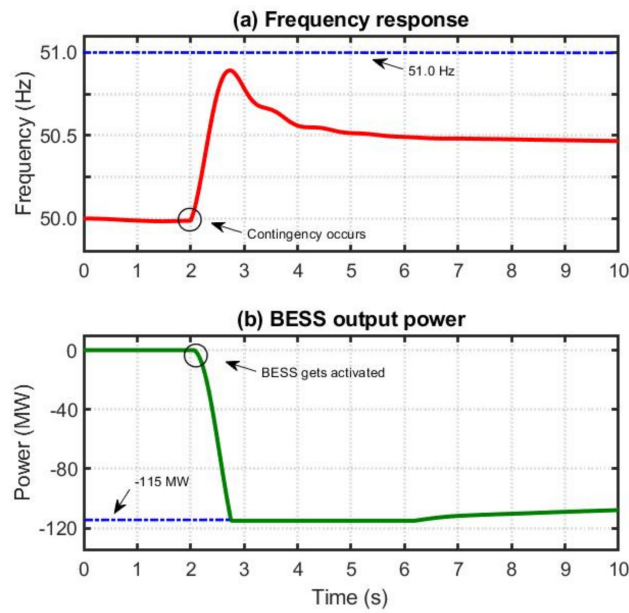**Figure 9.** Frequency responses and BESS output due to 400-MW interconnection trip in four-machine case.

Figure 10. Frequency responses and BESS output due to 400-MW interconnection trip in three-machine case.

4.2.2. System Performance in Case-2

In this case, the loss of a 450-MW interconnection is simulated. Following this contingency, system frequency starts to rise that eventually activates the BESS. As such, frequency escalation is stopped before the OFGS threshold. Frequency excursion and BESS output power curves are depicted in Figures 11–13 for five-machine, four-machine and three-machine scenarios, respectively. The corresponding frequency summits are 50.82 Hz, 50.88 Hz and 50.98 Hz. Moreover, from the frequency response curves, the respective ROCOFs are calculated as 0.92 Hz/s, 0.93 Hz/s and 0.95 Hz/s. Thus, the grid frequency stays below 51 Hz and ROCOF is less than 1 Hz/s when the 115-MW BESS is allocated. Therefore, the over-frequency incident is effectively controlled by deploying the proposed methodology.
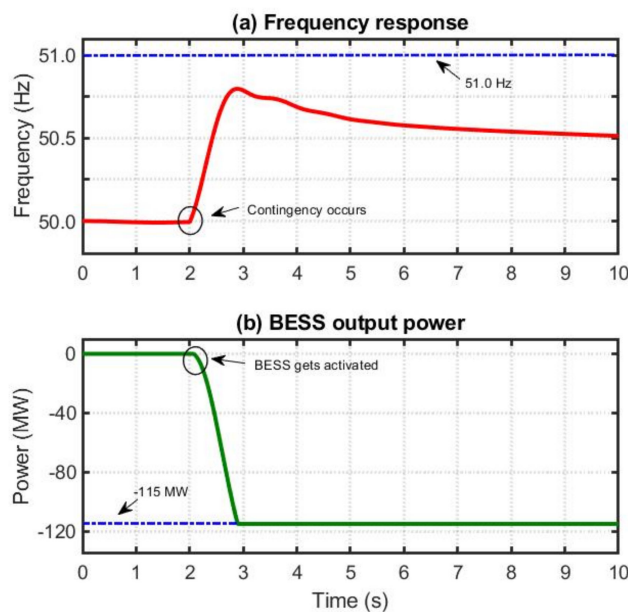

Figure 11. Frequency responses and BESS output due to 450-MW interconnection trip in five-machine case.
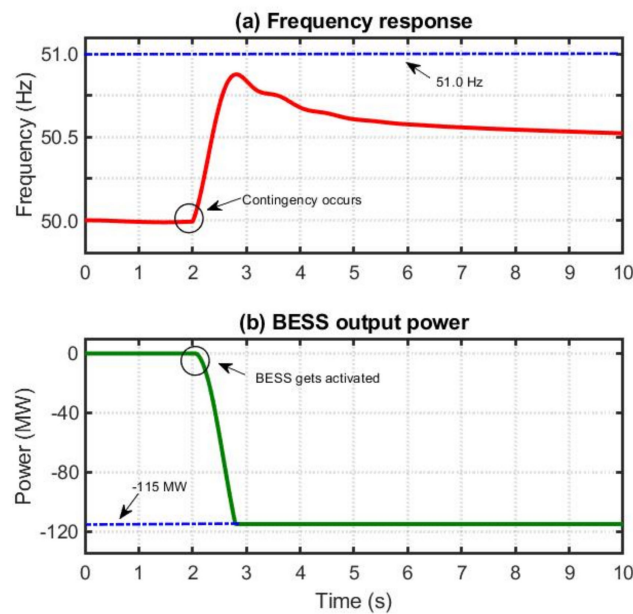
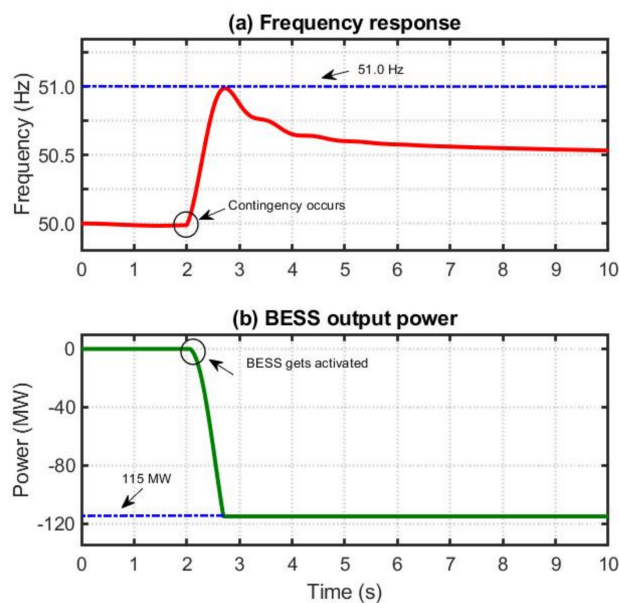**Figure 12.** Frequency responses and BESS output due to 450-MW interconnection trip in four-machine case.

Figure 13. Frequency responses and BESS output due to 450-MW interconnection trip in three-machine case.

4.2.3. System Performance in Case-3

It must be emphasized that the optimal BESS size is determined by considering the 450-MW interconnection trip. However, if the contingency size increases further, the system performance needs to be re-evaluated. To address this situation, the loss of 500-MW interconnection is taken into account. Since increasing BESS size causes financial concern, the 115-MW BESS is utilized while simulating the aforementioned contingency. Nevertheless, the OFGS scheme (briefly described in Table 4 in Section 4.3) may be activated in certain cases.

It is found that in the five-machine and four-machine cases, the frequency summits are 50.85 Hz, 50.97 Hz, respectively (Figures 14 and 15). Therefore, the OFGS mechanism is not triggered. However, in the three-machine case, the frequency summit is 51.10 Hz, as shown in Figure 16a Since system frequency crosses the 51-Hz threshold, the OFGS action is activated. It causes 150-MW generation

shedding, as depicted in Figure 16c Thus, the 115-MW BESS accompanied by a 150-MW generation cut is required when system inertia is relatively low. In addition, from the frequency excursion curves, ROCOFs are enumerated as 0.95 Hz/s, 0.96 Hz/s and 0.97 Hz/s in five-machine, four-machine and three-machine cases, respectively. This indicates that ROCOF stays below the permissible limit for all cases.
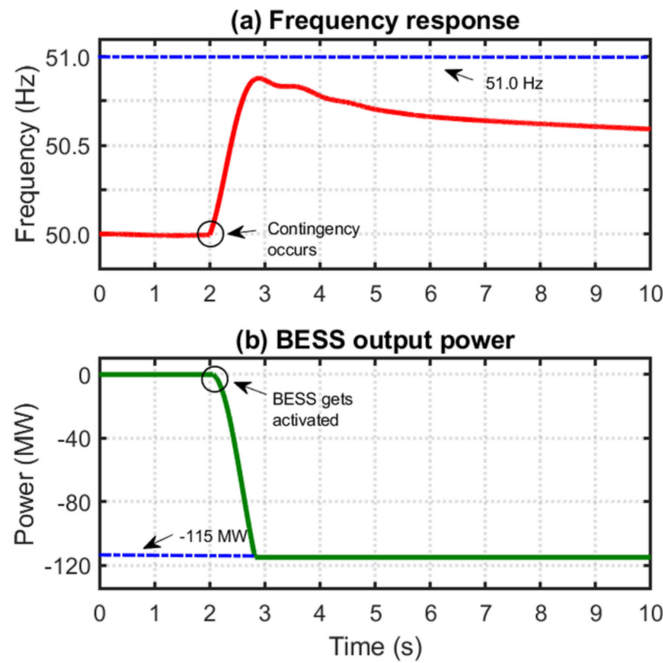

Figure 14. Frequency responses and BESS output due to 500-MW interconnection trip in five-machine case.
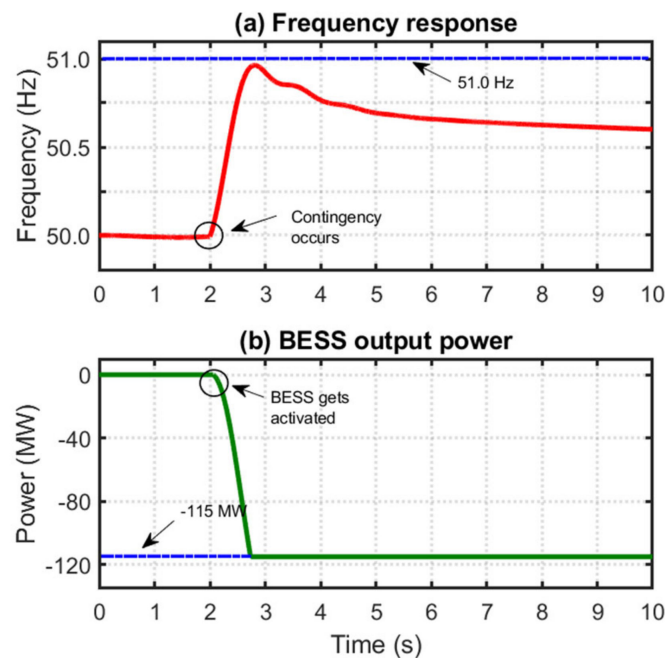

Figure 15. Frequency responses and BESS output due to 500-MW interconnection trip in four-machine case.
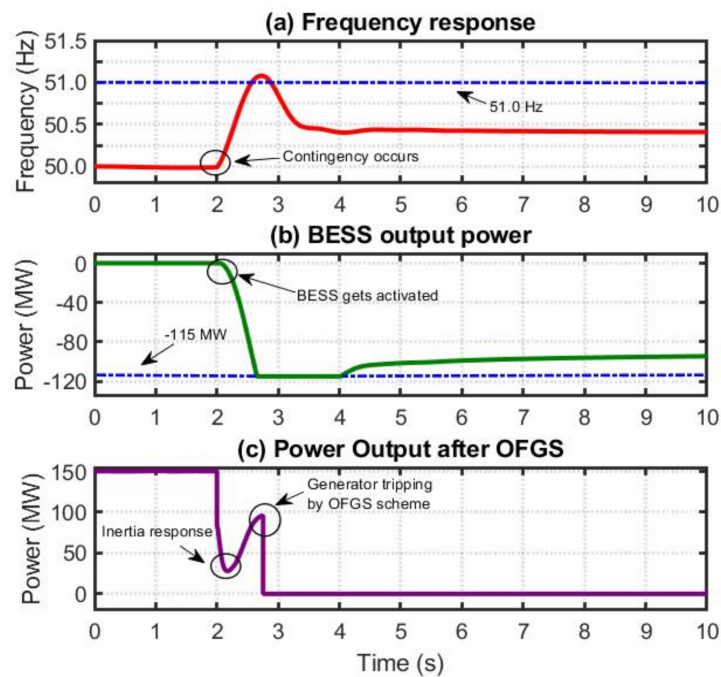
Figure 16. Frequency responses, BESS output and Over-Frequency Generator Shedding (OFGS) due to 500-MW interconnection trip in three-machine case.

4.3. Validation of the Proposed Methodology

To validate the proposed methodology, its performance is compared to that of the counterpart, i.e., without deploying BESS. When no BESS is incorporated, system has to solely rely on OFGS scheme to stop the frequency escalation. The OFGS scheme consists of three stages. In the first stage, one generator is cut at 51 Hz. Then, an additional generator is cut at 51.25 Hz while at 51.50 Hz, three generators are tripped to stop the over-frequency. Table 4 outlines an overview of the OFGS scheme used in this paper.

Table 4. Overview of OFGS scheme.

Description	Value
First generator tripping frequency threshold	51.00 Hz
Second generator tripping frequency threshold	51.25 Hz
Third generator tripping frequency threshold	51.50 Hz
Relay pick-up time	0.00005 s
Breaker time	0.083 s

In the following sub-sections, frequency response behaviors are comprehensively compared (with vs. without the BESS) for case-1, case-2 and case-3.

4.3.1. Performance Comparison in Case-1

In this case, frequency response is analyzed for the loss of 400-MW interconnection under power export conditions. When no BESS is utilized, frequency summits are found to be 50.91 Hz, 50.95 Hz and 50.98 Hz in five-machine, four-machine and three-machine cases, respectively. However, when the optimally sized BESS is connected, the corresponding summits reduce to 50.74 Hz, 50.81 Hz and 50.83 Hz. Therefore, the frequency peaks reduce by 0.17 Hz, 0.14 Hz and 0.15 Hz in five-machine, four-machine and three-machine cases, respectively. In addition, without BESS, the respective ROCOFs are 1.05 Hz/s, 1.15 Hz/s and 1.29 Hz/s. It indicates that before placing BESS, the ROCOF violates the

permissible limit of 1 Hz/s in all cases. Nevertheless, after placing the BESS, ROCOF is confined to 1 Hz/s in all machine cases. Therefore, it is evident that the proposed methodology is more effective to mitigate over-frequency. The frequency response curves are compared in Figure 17 for clearer observation.
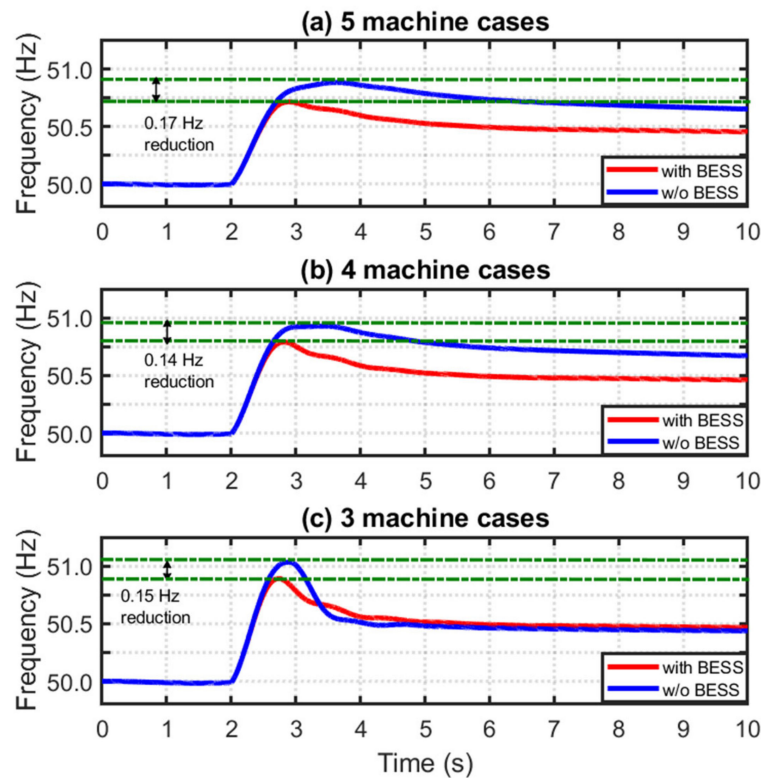

Figure 17. Performance comparison due to 400-MW interconnection trip: (**a**) five-machine case; (**b**) four-machine case; (**c**) three-machine case.

4.3.2. Performance Comparison in Case-2

In this case, the 450-MW interconnection trip is investigated. It is found that, without installing BESS, the frequency summits are 51 Hz, 51.02 Hz and 51.12 Hz when five machines, four machines and three machines are committed, respectively. Notably, the frequency exceeds the first threshold of the OFGS scheme. Consequently, 150-MW generation is shed in all three situations. On the other hand, when BESS is deployed the frequency summits are 50.82 Hz, 50.88 Hz and 50.98 Hz. Therefore, system frequency is arrested below the OFGS-triggering threshold. As a result, the system does not encounter any generation cut. In addition, the frequency summits decrease by 0.18 Hz, 0.14 Hz and 0.14 Hz in five-machine, four-machine and three-machine cases when the optimally sized BESS is connected.

Figure 18 shows a comparison of frequency response curves for a different number of online machines. Without BESS, ROCOFs are computed as 1.16 Hz/s, 1.26 Hz/s and 1.31 Hz/s in five-machine, four-machine and three-machine cases, respectively. It implies that ROCOF breaches the acceptable limit when only the OFGS scheme is utilized to stop over-frequency. However, when BESS is placed, ROCOF significantly reduces and resides below 1 Hz/s. In particular, BESS utilization yields 0.24 Hz/s, 0.33 Hz/s and 0.36 Hz/s reductions in system ROCOF during five-machine, four-machine and three-machine cases, respectively. Therefore, the proposed methodology stops system frequency below 51 Hz to avoid generation shedding and restricts ROCOF values to acceptable limits.
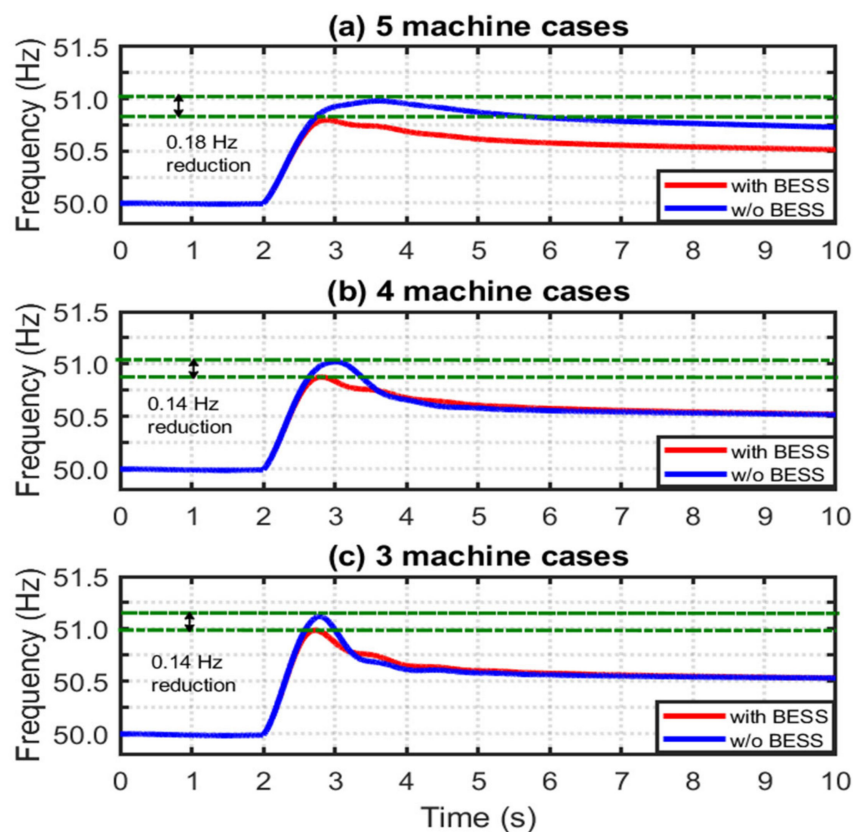
Figure 18. Performance comparison due to 450-MW interconnection trip: (**a**) five-machine case; (**b**) four-machine case; (**c**) three-machine case.

4.3.3. Performance Comparison in Case-3

This is a relatively high contingency scenario, where a 500-MW interconnection trip is simulated. Before utilizing BESS, the frequency summits are 51 Hz and 51.11 Hz in five-machine and four-machine cases, respectively. Since system frequency surpasses the OFGS triggering threshold, 15-MW generation is cut in both cases. However, in the three-machine case, the frequency summit is found to be 51.25 Hz. It causes the activation of the first and second stages of the OFGS scheme. As such, the network encounters 300-MW generation loss.

On the other hand, when BESS is placed, the frequency summits decrease. The values are 50.85 Hz, 50.97 Hz and 51.10 Hz in five-machine, four-machine and three-machine cases, respectively. Therefore, the corresponding reductions in frequency peaks are 0.15 Hz, 0.14 Hz and 0.15 Hz. Furthermore, the first stage of the OFGS scheme is activated only in the three-machine case, which causes a 150-MW generation cut (compared to the 300-MW cut without BESS). Figure 19 depicts the frequency response curves in various operating conditions.

Before incorporating BESS, ROCOFs are found to be 1.28 Hz/s, 1.33 Hz/s and 1.35 Hz/s in five-machine, four-machine and three-machine cases, respectively. Thus, ROCOF does not comply with the acceptable limit. However, after BESS is used, respective ROCOF decreases by 0.33 Hz/s, 0.37 Hz/s and 0.38 Hz/s. Eventually, the utilization of BESS brings down the ROCOF values to the allowable threshold.
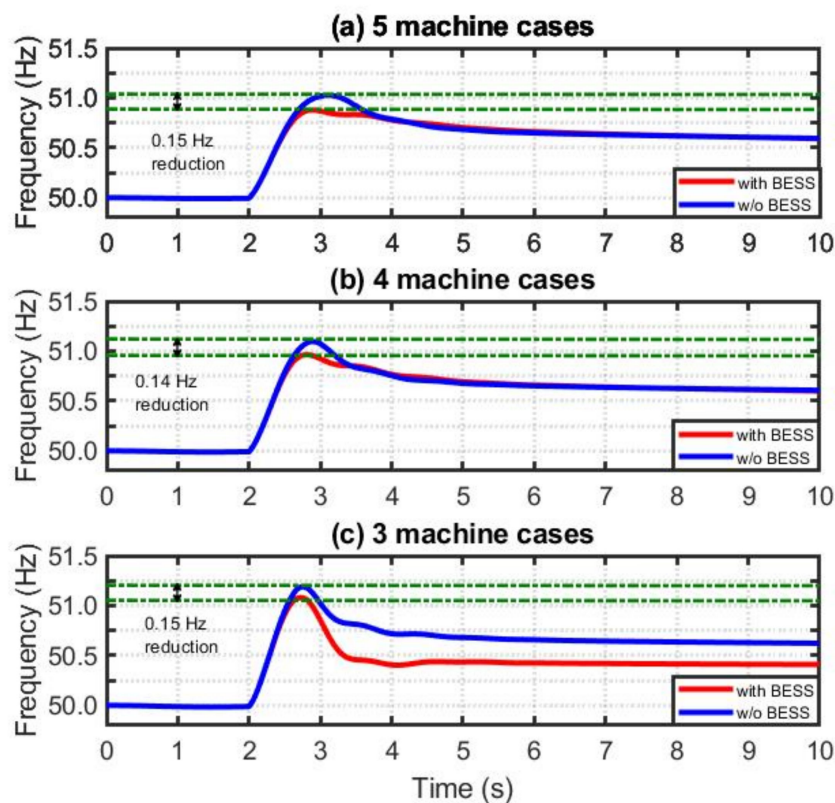
Figure 19. Performance comparison due to 500-MW interconnection trip: (**a**) five-machine case; (**b**) four-machine case; (**c**) three-machine case.

It can be revealed from the above analyses that the proposed BESS allocation technique provides a better performance compared to that of OFGS alone (i.e., no BESS). Therefore, the proposed methodology is found to be more effective to mitigate over-frequency in a low-inertia power system. For ease of comparison, Table 5 summarizes the performances of the two strategies.

Table 5. Summary of system performance.

Contingency Size (MW)	No. of Synchronous Generator	With BESS			Without BESS		
		Frequency Summit (Hz)	ROCOF (Hz/s)	OFGS Amount (MW)	Frequency Summit (Hz)	ROCOF (Hz/s)	OFGS Amount (MW)
400	5	50.74	0.88	0	50.91	1.05	0
	4	50.81	0.90	0	50.95	1.15	0
	3	50.83	0.92	0	50.98	1.29	0
450	5	50.82	0.92	0	51.00	1.16	150
	4	50.88	0.93	0	51.02	1.26	150
	3	50.98	0.95	0	51.12	1.31	150
500	5	50.85	0.95	0	51.00	1.28	150
	4	50.97	0.96	0	51.11	1.33	150
	3	51.10	0.97	150	51.25	1.35	300

4.4. Effectiveness of the Proposed Methodology with Load Variation

To demonstrate the effectiveness of the developed approach under various load conditions in Area-A, additional simulations are carried out. To this end, four new load levels viz. 1300 MW, 1400 MW, 1600 MW and 1700 MW are considered. Optimal BESS sizes are estimated following the loss

of the 450-MW interconnection trip to mitigate over-frequency events. Table 6 shows the results in different load scenarios.

Table 6. Optimal BESS sizes under different load levels.

Load in Area-A (MW)	Optimal BESS Size (MW)
1300	134
1400	125
1500	115
1600	106
1700	97

It can be noted that the required BESS size reduces with an increase in load. This is because under a relatively higher load, more synchronous generators are usually committed. Consequently, inertia and frequency control reserves increase. As a result, frequency response improves (i.e., peak frequency following a contingency reduces). Therefore, in high load conditions, the requirement of additional support from BESS to mitigate over-frequency is likely to decrease. The simulation results shown in Table 6 conform to the above-mentioned fundamental aspect. Thus, the proposed methodology is found to be effective with a variable load in the power-exporting zone.

4.5. Applicability of the Proposed Methodology under High PV Penetration

In this work, variable speed wind machines are considered, which are decoupled from the corresponding grid via power electronic converters. Consequently, these machines usually do not offer inertia and governor response to control system frequency. Likewise, PV generators are isolated from the grid though power electronics interfaces. Hence, traditionally, PV generators neither provide inertia nor primary frequency response [43,44]. Therefore, the nature of frequency control challenge during high PV penetration is the same as that of prolific wind penetration. Therefore, the proposed method of this paper can be applied to power systems with a lot of PV generation.

4.6. Further Insight into the Proposed Methodology

4.6.1. Superiority of the Proposed Siting and Sizing Approach

The most commonly used technique to mitigate over-frequency events is the utilization of the OFGS scheme. However, this approach causes the loss of a certain amount of generation. In addition, the tripping of a large generating unit may result in generation over-cuts. It may cause rapid frequency decline, which may lead to under-frequency load shedding in extreme cases [45]. Moreover, relay pick-up time and breaker time introduce several delays in OFGS operation [46].

In contrast, BESS is a fast frequency-responsive device that can be used to mitigate over-frequency without causing any loss of generation. Furthermore, in this paper, BESS is placed at the weakest bus to take care of voltage stability. Therefore, the superiorities of the proposed siting and sizing approach compared to the existing method are threefold: (i) it averts the loss of generation and generation over-cut, (ii) it provides a quick response to mitigate over-frequency events and (iii) it simultaneously ensures voltage and frequency stabilities in a low-inertia grid.

4.6.2. Pros and Cons of the Developed Method

The advantages of the proposed methodology are as follows.

- BESS is a fast frequency-responsive device. Its output can be changed from 0 to 100% of the rated capacity within a second based on frequency deviation. Therefore, unlike OFGS, BESS has no relay pick-up and breaker delays. This enables BESS to respond very quickly to mitigate the over-frequency phenomenon.

- BESS output can be changed smoothly. This implies that there is no possibility of over-reduction in generation when BESS is utilized. Therefore, the risk of unwanted under-frequency load shedding is averted.
- The siting and sizing techniques presented in this paper are generic in nature. Therefore, the proposed methodology can be applied to any power system to manage over-frequency events, especially under high renewable penetration.

The limitations of the proposed methodology are discussed below.

- The installation, operation and maintenance of BESS yield additional costs. Therefore, the widespread deployment of BESS is still not economically viable for many power systems, especially in underdeveloped countries.
- The optimization algorithm (PSO) used in this work is a meta-heuristic technique. Meta-heuristic techniques do not always guarantee global minima. To this end, the PSO algorithm is run multiple times until the outputs start to repeat. The output that provides the minimum objective function is considered as the final solution. However, the above procedure may introduce additional complexity into the computation process.

4.7. Potential of the Proposed Approach from Economic Perspective

In this research, conventional lithium-ion (Li-ion) batteries are deployed to mitigate over-frequency. Li-ion batteries have a very high energy density, fast response and long lifespan. Moreover, the efficiency of Li-ion batteries is very high. These advantages enable Li-ion batteries to be widely used in large power systems.

The typical installation cost of a Li-ion battery is 1200 USD/kW [47]. For instance, in the case of a large BESS with a capacity of 115 MW, the total installation cost will be MUSD138. Though this cost is relatively higher, it will be compensated considering the BESS lifetime of 20 years [47]. Furthermore, the usual operational cost of Li-ion batteries is 600 USD/kWh [47]. Notably, BESS provides support only for a short duration during over-frequency events. Hence, it is likely that the total operational cost will not introduce any financial burden to network operators. Therefore, considering the above aspects, a large BESS can be economically viable in large power systems. Likewise, from an economic perspective, the proposed approach has significant potential to deliver worthwhile outcomes.

5. Conclusions

This paper proposes a methodology for the siting and sizing of BESS to mitigate the over-frequency problem in a low-inertia power system. To this end, a frequency-responsive BESS is placed in the bus with the lowest reactive power margin (i.e., at the weakest bus). By doing so, voltage stability is retained along with frequency stability following a contingency. Then, an optimization model is formulated to determine the most appropriate size of BESS for alleviating over-frequency. The proposed methodology applied to a low-inertia power system consists of a few synchronous generators and high wind penetration. The optimal size of BESS is evaluated for a 450-MW interconnection trip by taking this as a baseline contingency. The optimization model results in a BESS size of 115 MW, which is eventually connected to the most voltage-sensitive bus. Furthermore, extensive simulations are carried out in various inertia levels for different magnitudes of contingencies to explore the effectiveness of the developed method.

It is found that, following the loss of 400-MW and 450-MW interconnections under power export conditions, the optimally sized BESS successfully stops the frequency escalation before the OFGS scheme is activated. Over-frequency generator shedding only occurs when a 500-MW contingency is considered and three generators are online. Furthermore, the ROCOFs are confined to the acceptable limit (i.e., less than 1 Hz/s) in all cases. To validate the proposed methodology, its performance is compared to the condition when no BESS is utilized. It is noted that frequency summits (i.e., frequency peaks) and ROCOFs significantly reduce when BESS is deployed. In addition, the amount of generation

shedding considerably decreases due to BESS incorporation. Therefore, the proposed methodology effectively mitigates the over-frequency phenomenon. It also yields better performances compared to its counterpart. Finally, it is worth mentioning that the developed technique can be applied to any power system to manage the over-frequency challenge, especially under high renewable penetration.

References

1. Yu, D.; Zhang, W.; Li, J.; Yang, W.; Xu, D. Disturbance Observer-Based Prescribed Performance Fault-Tolerant Control for a Multi-Area Interconnected Power System with a Hybrid Energy Storage System. *Energies* **2020**, *13*, 1251. [CrossRef]
2. Shazon, M.N.H.; Ahmed, H.M.; Masood, N.A. Over-Frequency Mitigation Using Coordinated Generator Shedding Scheme in a Low Inertia Power System. In Proceedings of the IEEE Region 10 Symposium, (TENSYMP), Dhaka, Bangladesh, 5–7 June 2020; pp. 560–563.
3. Peña Asensio, A.; Gonzalez-Longatt, F.; Arnaltes, S.; Rodríguez-Amenedo, J.L. Analysis of the Converter Synchronizing Method for the Contribution of Battery Energy Storage Systems to Inertia Emulation. *Energies* **2020**, *13*, 1478. [CrossRef]
4. Alsharafi, A.S.; Besheer, A.H.; Emara, H.M. Primary frequency response enhancement for future low inertia power systems using hybrid control technique. *Energies* **2018**, *11*, 699. [CrossRef]
5. Statistics Time Series, Irena.org. 2020. Available online: https://www.irena.org/Statistics/View-Data-by-Topic/Capacityand-Generation/Statistics-Time-Series (accessed on 7 July 2020).
6. Yan, R.; Saha, T.K.; Modi, N.; Masood, N.A.; Mosadeghy, M. The combined effects of high penetration of wind and PV on power system frequency response. *Appl. Energy* **2015**, *145*, 320–330. [CrossRef]
7. Zaman, M.S.; Irfan, M.; Ahmad, M.; Mazzara, M.; Kim, C.H. Modeling the Impact of Modified Inertia Coefficient (H) due to ESS in Power System Frequency Response Analysis. *Energies* **2020**, *13*, 902. [CrossRef]
8. AEMO. Update to Renewable Energy Integration in South Australia. 2016. Available online: http://www.aemo.com.au (accessed on 7 July 2020).
9. Yang, F.; Su, Y.H.; Zhao, S.Q.; Song, Y.T.; Mei, Y.; Wang, Q.; Zhang, Z.Q. Research on over Frequency Generator Tripping Configuration Scheme of Regional Grid in Infirm Interconnections and Small Capacity. *Appl. Mech. Mater.* **2013**, *336*, 1174–1179. [CrossRef]
10. Zhang, Z.; Li, X.; Huang, Z. Simulation and analysis of over Frequency generator tripping for Guizhou isolated power system. *Mod. Electr. Power* **2008**, *25*, 31–34.
11. Yang, F.; Zhang, Z.; Zhao, S.; Wu, L.; He, J. Configuration scheme of over-Frequency tripping and coordination with overspeed protection controller (OPC) of regional grid. *Electr. Power* **2013**, *46*, 64–68.
12. Moutis, P.; Hatziargyriou, N.D. Decision trees-aided active power reduction of a virtual power plant for power system over-frequency mitigation. *IEEE Trans. Ind. Inf.* **2014**, *11*, 251–261. [CrossRef]
13. Mashhour, E.; Moghaddas-Tafreshi, S.M. Bidding strategy of virtual power plant for participating in energy and spinning reserve markets—Part I: Problem formulation. *IEEE Trans. Power Syst.* **2010**, *26*, 949–956. [CrossRef]
14. Strbac, G.; Jenkins, N.; Green, T.; Pudjianto, D. *Review of Innovative Network Concepts*; DG GRID Project Report; European Commission: Petten, The Netherlands, 2006.
15. AEMO. South Australia—Power System Operation as a Viable Island. 2018. Available online: http://www.aemo.com.au (accessed on 8 July 2020).
16. Carpinelli, G.; Di Fazio, A.R.; Khormali, S.; Mottola, F. Optimal sizing of battery storage systems for industrial applications when uncertainties exist. *Energies* **2014**, *7*, 130–149. [CrossRef]
17. Abdulgalil, M.A.; Khalid, M.; Alismail, F. Optimal Sizing of Battery Energy Storage for a Grid-Connected Microgrid Subjected to Wind Uncertainties. *Energies* **2019**, *12*, 2412. [CrossRef]

18. Kim, Y.S.; Hwang, C.S.; Kim, E.S.; Cho, C. State of charge-based active power sharing method in a standalone microgrid with high penetration level of renewable energy sources. *Energies* **2016**, *9*, 480. [CrossRef]

19. Fiorini, L.; Pagani, G.A.; Pelacchi, P.; Poli, D.; Aiello, M. Sizing and siting of large-scale batteries in transmission grids to optimize the use of renewables. *IEEE J. Emerg. Sel. Top. Circuits Syst.* **2017**, *7*, 285–294. [CrossRef]

20. Pandžić, H.; Wang, Y.; Qiu, T.; Dvorkin, Y.; Kirschen, D.S. Near-optimal method for siting and sizing of distributed storage in a transmission network. *IEEE Trans. Power Syst.* **2014**, *30*, 2288–2300. [CrossRef]

21. Ramírez, M.; Castellanos, R.; Calderón, G.; Malik, O. Placement and sizing of battery energy storage for primary frequency control in an isolated section of the Mexican power system. *Electr. Power Syst. Res.* **2018**, *160*, 142–150. [CrossRef]

22. Knap, V.; Chaudhary, S.K.; Stroe, D.I.; Swierczynski, M.; Craciun, B.I.; Teodorescu, R. Sizing of an energy storage system for grid inertial response and primary frequency reserve. *IEEE Trans. Power Syst.* **2015**, *31*, 3447–3456. [CrossRef]

23. Tang, Z.X.; Lim, Y.S.; Morris, S.; Yi, J.L.; Lyons, P.F.; Taylor, P.C. A comprehensive work package for energy storage systems as a means of frequency regulation with increased penetration of photovoltaic systems. *Int. J. Electr. Power Energy Syst.* **2019**, *110*, 197–207. [CrossRef]

24. Oudalov, A.; Chartouni, D.; Ohler, C. Optimizing a battery energy storage system for primary frequency control. *IEEE Trans. Power Syst.* **2007**, *22*, 1259–1266. [CrossRef]

25. Nick, M.; Cherkaoui, R.; Paolone, M. Optimal siting and sizing of distributed energy storage systems via alternating direction method of multipliers. *Int. J. Electr. Power Energy Syst.* **2015**, *72*, 33–39. [CrossRef]

26. Babacan, O.; Torre, W.; Kleissl, J. Siting and sizing of distributed energy storage to mitigate voltage impact by solar PV in distribution systems. *Sol. Energy* **2017**, *146*, 199–208. [CrossRef]

27. Shayesteh, E.; Gayme, D.F.; Amelin, M. System reduction techniques for storage allocation in large power systems. *Int. J. Electr. Power Energy Syst.* **2018**, *95*, 108–117. [CrossRef]

28. Thrampoulidis, C.; Bose, S.; Hassibi, B. Optimal placement of distributed energy storage in power networks. *IEEE Trans. Autom. Control* **2015**, *61*, 416–429. [CrossRef]

29. Parker, C.J.; Morrison, I.F.; Sutanto, D. Application of an optimisation method for determining the reactive margin from voltage collapse in reactive power planning. *IEEE Trans. Power Syst.* **1996**, *11*, 1473–1481. [CrossRef]

30. Van Cutsem, T. A method to compute reactive power margins with respect to voltage collapse. *IEEE Trans. Power Syst.* **1991**, *6*, 145–156. [CrossRef]

31. Canizares, C.A.; Alvarado, F.L. Point of collapse and continuation methods for large ac/dc systems. *IEEE Trans. Power Syst.* **1993**, *8*, 1–8. [CrossRef]

32. Ajjarapu, V.; Christy, C. The Continuation Power Flow: A Tool for Steady State Voltage Stability Analysis. *IEEE Trans. Power Syst.* **1992**, *7*, 416–423. [CrossRef]

33. Lian, S.; Minami, S.; Morii, S.; Kawamoto, S. Analysis method of voltage stability for bulk power system by PV and QV curves considering dynamic load. In Proceedings of the 2009 IEEE/PES Power Systems Conference and Exposition, Washington, DC, USA, 15 March 2009; pp. 1–6.

34. Chiang, H.D.; Flueck, A.J.; Shah, K.S.; Balu, N. CPFLOW: A practical tool for tracing power system steady-state stationary behavior due to load and generation variations. *IEEE Trans. Power Syst.* **1995**, *10*, 623–634. [CrossRef]

35. Eckroad, S. *EPRI-DOE Handbook of Energy Storage for Transmission & Distribution Applications*; US Dept. of Energy: Washington, DC, USA, 2003; pp. 349–372.

36. DNV KEMA Energy & Sustainability. RoCoF an Independent Analysis on the Ability of Generators to Ride through Rate of Change of Frequency Values up to 2Hz/s. 2013. Available online: http://www.eirgridgroup.com/sitefiles/library/EirGrid/DNV_KEMA_Report_RoCoF_20130208final_.pdf (accessed on 10 June 2020).

37. Kennedy, J.; Eberhart, R. Particle swarm optimization. In Proceedings of the ICNN'95—International Conference on Neural Networks, Perth, Australia, 27 November 1995; Volume 4, pp. 1942–1948.

38. Pyswarm. 2013–2014. Available online: https://pythonhosted.org/pyswarm/ (accessed on 14 January 2020).

39. Gibbard, M.; Vowles, D. *Simplified 14-Generator Model of the SE Australian Power System*; Revision 3; The University of Adelaide: Adelaide, Australia, 2010.

40. AEMO. Interconnector Capabilities for the National Electricity Market. 2017. Available online: https://www.aemo.com.au/-/media/Files/Electricity/NEM/Security_and_Reliability/Congestion-Information/2017/Interconnector-Capabilities.pdf (accessed on 23 August 2020).
41. PSS®E, Power System Simulator for Engineering. 2017. Available online: http://www.energy.siemens.com/hq/en/services/powertransmission-distribution/power-technologies-international/softwaresolutions (accessed on 2 January 2020).
42. AEMC. Frequency Operation Standards. 2020. Available online: https://www.aemc.gov.au/australias-energy-market/market-legislation/electricity-guidelines-and-standards/frequency-0 (accessed on 30 July 2020).
43. You, S.; Liu, Y.; Zhang, X.; Su, Y.; Wu, L.; Liu, Y.; Hadley, S. Impact of high PV penetration on US eastern interconnection frequency response. In Proceedings of the 2017 IEEE Power & Energy Society General Meeting, Chicago, IL, USA, 16 July 2017; pp. 1–5.
44. Masood, N.; Yan, R.; Saha, T.K. Cascading Contingencies in Low Inertia Power Systems: Frequency Response Challenges and a Potential Solution. Proceedings of 2017 the IEEE Power & Energy Society General Meeting, Chicago, IL, USA, 16 July 2017; pp. 1–5.
45. Guo, Y.; Nan, H.; Guan, X.; Wu, L. Discussion on the Over-frequency Generator Tripping Scheme of the Power Grid. *JPhCS* **2018**, *1072*, 012010. [CrossRef]
46. Samaan, N.; Dagle, J.; Makarov, Y.; Diao, R.; Miller, L.; Wang, S.; Vyakaranam, B.; Nguyen, T.; Tuffner, F.; Pai, M.; et al. *Dynamic Contingency Analysis Tool–Phase 1*; Report 24843; Pacific Northwest National Laboratory: Richland, WA, USA, 2015.
47. Farhadi, M.; Mohammed, O. Energy storage technologies for high-power applications. *IEEE Trans. Ind. Appl.* **2015**, *52*, 1953–1961. [CrossRef]